Developments in the Built Environment 14 (2023) 100158

Contents lists available at ScienceDirect

Developments in the Built Environment

journal homepage: www.sciencedirect.com/journal/developments-in-the-built-environment

Experimental investigations of power-actuated fastenings in TRC

A.D. Langenbeck [a,b], P. Spyridis [a,*], M. Beßling [a], J. Orlowsky [a]

[a] TU Dortmund University, Faculty of Architecture and Civil Engineering, August-Schmidt-Str. 8, 44221, Dortmund, Germany
[b] RWTH Aachen University, Institute of Energy Efficiency and Sustainable Building, Mathieustr. 30, 52074, Aachen, Germany

ARTICLE INFO

Keywords:
Textile reinforced concrete
Direct fastenings
Power actuated fastenings
Façade anchorage

ABSTRACT

In this study we investigate the application of direct fastenings in textile-reinforced concrete for the first time in international research. This efficient combination is promising regarding sustainability and load-bearing reliability due to the fine-grained material structure. We aim to assess the system's feasibility and establish the most favourable framework of practice. Within our test series, we modify the concrete strength, the number of textile layers, the type of textile and the setting process. The most promising results were achieved when using three layers of a symmetric textile regarding geometry and tensile strength without executing a predrilling. While using higher-strength concrete leads to a total load-bearing capacity of up to 7 kN, this implies lower visual quality compared to lower-strength concrete. The latter case, with an average nail performance of over 4 kN, indicates that the proposed fastening-material-combination is highly promising regarding future use cases.

1. Introduction

1.1. Motivation, research significance and structure of paper

Research into the material defined as Textile-reinforced Concrete (TRC) has been ongoing since the 1990s [Scheerer, 2015]. A decisive advantage of this composite construction material, as described by Curbach and Jesse [Curbach and Jesse, 2009], is the possibility to minimise the dimensions of structural components and thus their self-weight, compared to typical reinforced concrete elements. The carbon fibre-based textile reinforcement has a substantially higher strength and hence a smaller required cross-section compared to standard steel reinforcement. Besides, it is not affected by corrosion, and it poses much higher durability. Consequently, a minimal concrete cover is required (both for bond and corrosion resistance purposes), and structural elements can be dimensioned with a thickness of even 10 mm [Curbach and Jesse, 2009]. The material can then lead to up to 86% reduction of material resources in relation to conventional concrete and much lower total CO2-equivalent emissions than steel-reinforced concrete over the entire life cycle of comparable building components [Haist et al., 2022]. At the same time, the very special nature of the material requires the re-examination of conventional fastening systems or the development of new methods [Hoepfner et al., 2021]. One approach to improving sustainability can be to minimise the material volume and production complexity of fastening products and, at the same time, the energy resources of the fastening process itself. One such efficient technology is the direct fastening of nails.

Besides sustainability, further positive characteristics of this fastening method are the very fast – virtually instant – installation and the overall reduced labour time, the absence of noise, dust, and vibrations (compared to e.g. hammer drilling), and the independence from weather conditions, specially trained and qualified labour, and power supply on-site [Beck et al., 2019]. On the other side, the highly dynamic installation characteristics may lead to a substantial variability of the load resistance, as discussed by Patzak [Patzak, 1979]. Nails for use in concrete may have a diameter and embedment depth of up to approximately 5 and 40 mm, respectively. The fact that concrete is quite inhomogeneous at this scale can lead to dislocation and distortion of the nail (e.g. due to encountering a tough large aggregate), or to local cracking and spalling around the nail (e.g. due to a crack developing in the matrix). This, in turn, may significantly reduce the load-bearing capacity or even cause a setting failure. Fig. 1 illustrates this phenomenon. Given the abovementioned sustainability benefits as well as the fine texture and homogeneity of TRC [Lieboldt, 2015] [Beßling et al., 2022a], its combination with direct fastenings may render an interesting solution, which forms the motivation for this study.

The remaining part of the introduction below briefly presents a theoretical background on the structural performance of TRC and existing knowledge on fastenings in TRC. Also, the technological and engineering fundamentals of direct fastenings are discussed. The next

* Corresponding author.
E-mail address: panagiotis.spyridis@tu-dortmund.de (P. Spyridis).

https://doi.org/10.1016/j.dibe.2023.100158
Received 9 January 2023; Received in revised form 27 March 2023; Accepted 31 March 2023
Available online 18 April 2023

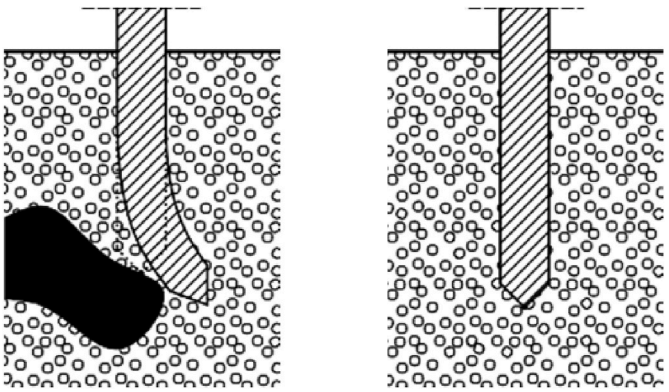

Fig. 1. Schematic representation of: Nail with reduced load-bearing capacity when deflected by aggregate in normal concrete (left), and nail in homogeneous concrete with fine aggregates (right).

section describes the configuration of experimental investigations performed at TU Dortmund University comprising 60 detailed setting and pull-out tests. The results are demonstrated and discussed in a separate subsequent section, with focus on the visual appearance of the fastened panels (pertinent to the serviceability limit state), as well as the connection's structural performance (pertinent to ultimate limit state). Finally, conclusions regarding the research questions noted in the previous section are summarised and an applicability spectrum of the TRC and direct fastening system is disclosed for the first time in scientific literature worldwide.

1.2. Principles of textile reinforced concrete

Methods for producing textile reinforced concrete panels include lamination at the desired distance [Beßling et al., 2022a] with alternate layering of concrete and textile or a casting process [Walther et al., 2014] using a spacer system to secure the textile layers are at predefined positions in a formwork followed by casting of fine-grained concrete. The composite load-bearing behaviour of the material under uniaxial tensile stress is to some extent resembling this of normal reinforced concrete [Lorenz et al., 2013; Lorenz, 2015]: Initially, the load transfer occurs predominantly via the concrete matrix, namely at *State I* which is linear-elastic. As crack appear, the transition to *State IIa* ensues and the force flow is bridged and introduced into the concrete matrix via the concrete-textile bond near the crack tips until the crack width, and the associated transmitted forces are below the tensile strength of the concrete. The bond-slip performance then depends on both the textile characteristics (mainly geometry and impregnation agent) and the concrete mechanical properties and force transfer is achieved mainly through friction and to a lesser grade mechanical anchorage of the textile's lateral strands [Beßling and Orlowsky, 2022]. In *State IIb*, material deformation continues via the elastic strain of the textile until the textile fails under brittle tension [Lorenz et al., 2013; Lorenz, 2015]. It is hence noted that a certain level of cracking is inherent to the load-bearing mechanism of TRC under (direct or flexural) tension.

1.3. Background knowledge on fastenings in textile reinforced concrete

TRC was first used in façade construction, with the first approved TRC panel developed in Germany [Hegger et al., 2005]. Fastening requirements specified by the technical approval organization [Deutsches Institut für Bautechnik, 2019] prescribe casting four internally threaded sleeves into the panel's back and using special screws and support profiles or agraffes to fasten them to the substructure. An alternative approved system such panels is achieved by means of a shallow post-installed undercut anchor at least four fixing points [Deutsches Institut für Bautechnik, 2021a]. Another available approved system for fastening thin TRC façade plate elements, uses cast-in mechanical anchorages which can be integrated into a broad typology of substructure walls [Deutsches Institut für Bautechnik, 2021b].

Curbach and Speck [Curbach and Speck, 2008] tested cast-in headed steel dowels in glass-fibre-textile-reinforced plates. These investigations established basic influences on the concrete failure mechanism and resistance, and confirmed that the load-bearing capacity of the anchor depends on the flexural strength of the test specimen. An increasing of reinforcement quota in the specimen also led to an increase in the load-bearing capacity of the anchor, and additional reinforcement layers did not influence the anchorage resistance but only the ductility. As a reference for the study herein, tests with an anchor embedment depth of about 9 mm at a diameter of 20 mm in a 16 mm thick, single-layer reinforced slab, pull-out forces under uniaxial tension of around 2 kN could be achieved [Curbach and Speck, 2008]. Investigations on post-installed systems with undercut and bonded anchors were carried out by Höpfner et al. [Hoepfner et al., 2021] in embedment depths between 10 and 25 mm were tested. The resulting range of anchor tensile resistance was between 2.0 and 6.0 kN, with a strong dependence on the embedment depth.

1.4. Installation and bearing performance of direct fastenings

The engineering and technological fundamentals of direct fastening technology and engineering are presented by Beck et al. [Beck et al., 2019]. This fastening method relies on dynamic penetration of high-strength steel nails at a speed of 50–200 m/s, using pistons actuated through gun-powder cartridges, pneumatic pressure, or electromechanically controlled springs. In addition, a distinction is made between direct fastenings without or with guidance predrilling. In the case of predrilling a short pilot hole with a diameter approximately equal to the nail and a depth of 5–15 mm is realised in advance of driving the nail in concrete. This minimises the risk of setting defects, but in turn of course requires more time and effort for the setting procedure [Beck, 2012].

The anchoring mechanism and load transfer rely on three distinct bearing effects: clamping, sintering, and interlocking [Gerber, 1987], [Hilti Corporation, 2021]. Upon nail penetration into the concrete, the concrete is locally displaced in the radial direction transversely to the nail axis, resulting in a clamping action. The high setting speeds cause friction between the nail and the concrete, resulting in heat release and the development of high temperatures [Patzak, 1979]. Sintering occurs when the top layer of the nail at the friction interface with concrete melts and solidifies immediately after setting [Gerber, 1987]. The sintering of the material then creates a roughened, uneven nail surface that interlocks with the surrounding concrete. Sintering and interlocking occur mainly at the tip of the nail, which leads to adhesion or bonding, and clamping develops at a depth of approximately 2–3 nail diameters from the surface. The load-bearing mechanism relies on a combination of the effects mentioned above. In axial load tests, failure usually occurs due to concrete breakout starting at the nail tip region sintered with the concrete, provided that this connection has an overall higher strength than the concrete matrix tensile resistance. A loss of bond and pull-out failure may also occur. The mode of failure the overall load-bearing performance, besides local installation defects, are further related to the nail penetration depth, the edge distance and nail spacing, and the concrete properties, particularly the concrete strength and the aggregate toughness and size distribution [Gerber, 1987], [Hilti Corporation, 2021]. Patzak also investigated the influence of cracks on the load-bearing capacity of nails in normal concrete which yields the conclusion that cracks generated artificially after the installation lead to a reduction of the load-bearing capacity by up to 42% and 70%, for a crack width of 0.1 mm and 0.4 mm respectively, as compared to uncracked concrete [Patzak, 1979]. Furthermore, the study proposes that nails set prior to the formation of cracks exhibit a more favourable behaviour than those placed in pre-existing cracks, indicating the

Table 1
Nomenclature of the main experiments including selectable options.

Compressive strength of the concrete	Textile type/ geometry	No. Of textile layers	Predrilling depth
40 N/mm2	HTC **10/15**-40	**3** layers	**0** mm
80 N/mm2	HTC **21/21**-40	**1** Layer	**7** mm

influences of different tension stress patterns of the concrete surface in the two situations.

In the same study, Patzak [Patzak 1979] proposes that a very substantial variability underlies the load-bearing resistance of direct fastenings in normal concrete. As indicated, the average resistance of nails with a penetration depth of 27 mm is approximately 4.50 kN, whereas the variation coefficient is around 40% and higher for cracked concrete. In addition to this, a number of installation failures is observed (i.e. a resistance equal to nil). With traditional statistics this would lead to a nominal/characteristic value of approximately 0.20 kN, i.e. less than 20 times smaller than the mean value. In order to be able to reach acceptable overall nominal resistance values, Patzak proposes a design concept for lightweight suspended ceilings based on multiple fastening points with the ability to redistribute loads with each other in case some points in a group exhibit actually very low resistances without violating the overall system requirements [Patzak 1979]. This concept is currently valid for the design of fastenings governed by significant uncertainties in the performance and it accepts local defects or damage, particularly for non-structural applications [EOTA, 2018] and normal cracked and uncracked concrete.

2. Experimental investigations

2.1. Nomenclature and geometry configurations

The labeling of the experiments is done according to the properties shown in Table 1. The options listed are selected in any combination. The configurations A-40-10/15-3-0 and A-80-10/15-3-0 represent the two reference configurations. The suffix WH signifies a repetition of tests for a configuration that was investigated more closely and more results were required. Some of the 3-layer configurations were tested with and without predrilling. Fig. 2 shows the tested panel configurations schematically.

2.2. Materials

2.2.1. Concrete

In the experimental campaign, two strength levels were used, namely 40 and 80 MPa following DIN EN 12390–2, i.e. measured on a dry cube with an edge length of 150 mm [DIN EN 12390–2, 2019]. As part of the mix development, prisms were produced and tested following DIN EN 196–1 with varying mixing processes [DIN EN 196-1, 2016]. The conversion of the cube compressive strength from a cube with an edge length of 40 mm to a cube with an edge length of 15 cm is carried out by means of the factor 0.86, which also agrees well with previous research studies at the Department of Building Materials, TU Dortmund University. The bending tensile strength noted herein is not converted, and it is based on 3-point bending tests of 40x40 × 160 mm prisms according to [DIN EN 196-1, 2016]. Fresh concrete spread was measured in adherence to [DIN EN 1015-3, 2007] to check its workability and 15.5–17.0 cm was achieved in all measured cases after 20 min. The mix compositions are shown in Table 2.

2.2.2. Textile reinforcement

The specimens include the two textiles shown in Fig. 3, namely HTC 10/15–40 and HTC 21/21–40. Both textiles consist of carbon fibres, and they are soft-impregnated [Beßling et al., 2022b] with styrene-butadiene. The textiles are delivered in rolls, with the rolling longitudinal direction (warp) corresponding to the indicated 0° direction [Hitexbau GmbH, n.Da; Hitexbau GmbH, n.D.b]. The main differences of the two textile types result from the textile geometry and the direction-dependent strength of the textiles. HTC 10/15–40 is characterised by a rectangular mesh geometry of a 15 by 10 mm clearance. The degree of reinforcement is also different in the two directions: the warp cross-section has 48 thousand filaments (48k) with a total area of 142 mm^2/m and a tensile strength of 362.2 kN/m. Transversely, the cross-section is a 12k with an area of 25 mm^2/m with a tensile strength of 71.1 kN/m. HTC 21/21–40 has a quadratic mesh with 48k and 71 mm^2/m strands at a 22 mm clearance, with a 169 kN/m average tensile strength. The parameter $k_{A,eff}$ represents a tensile strength reduction (concerning a splitting crack in the concrete) factor depending on the ratio of textile-reinforcement in-plane area to the concrete influence area, and hence the interface load-bearing performance, based on the concept proposed in [Ortlepp, 2007]. The values of 0.64 for and 0.71 were determined for HTC 10/15–40 and HTC 21/21–40, respectively.

2.3. TRC specimens

2.3.1. Production and curing

The TRC panels were produced through a horizontal casting process, aspects of which are shown in Fig. 4. To secure its position during casting, the textile was clamped at the edges of the formwork. Spacers were deliberately omitted to exclude a possible influence on the nail setting. In order to produce the concrete, the dry components were weighed and homogenised, water and superplasticiser were mixed beforehand, added to the dry components and mixed for approx. Another 5 min. Vibration time and formwork filling were regulated visually. The vibration process was generally kept short (approximately 30 s) to avoid segregation. A set of material tests prisms was nearly produced and stored in the same process as the panels. Another set was produced following DIN EN 196 [DIN EN 196–1] and stored according to [DIN 12390] (dry storage). The latter specimens were subjected to immersed and climate chamber curing. The TCR panels and the similarly produced set of prisms were placed together in the non-conditioned indoor environment of the laboratory, covered with a canvas until stripping and then wrapped in a wet canvas and tarpaulin in otherwise free air. Nail setting and its evaluation was always carried out on the 28th or 29th day.

2.4. Nail product and setting process

The used fastener was the Hilti X–U 27 P8, with 4 mm diameter and 27 mm shank length, installed by use of the respective Hilti DX 5-F8 powder-actuated setting tool. A metal adapter with a 4 mm hole at the fastening point and a sheet thickness of 2 mm was designed and produced at the Institute of Construction Research at the TU Dortmund in order to simulate a realistic fixture element and also to apply the axial test load. Predrilling of a 4 mm diameter and 7 mm depth was carried out by use of a rotating drill bit without percussion. The setting energy is adjusted via the cartridge selection (colour) and the energy fine-tuning on the setting device (number). The approximate setting energies (E_{set}) applied are shown in Table 3, and it was established based on a series of preliminary tests. These initial tests followed a trial-and-error approach in a structured event-tree sequence until an optimum setting with the minimum overall panel damage was achieved, but they are not further reported herein. Fig. 5 shows detail of the nail and the adapter and the specimen configuration with the target positioning of the nail. The specimen is placed on a 1 cm thick elastomer with a hardness of 65 ± 5 at the Shore A scale.

2.5. Pull-out tests

The load capacity of the nails was tested in terms of axial tensile load, as shown in Fig. 6. The load cell is placed centrally on the wooden frame

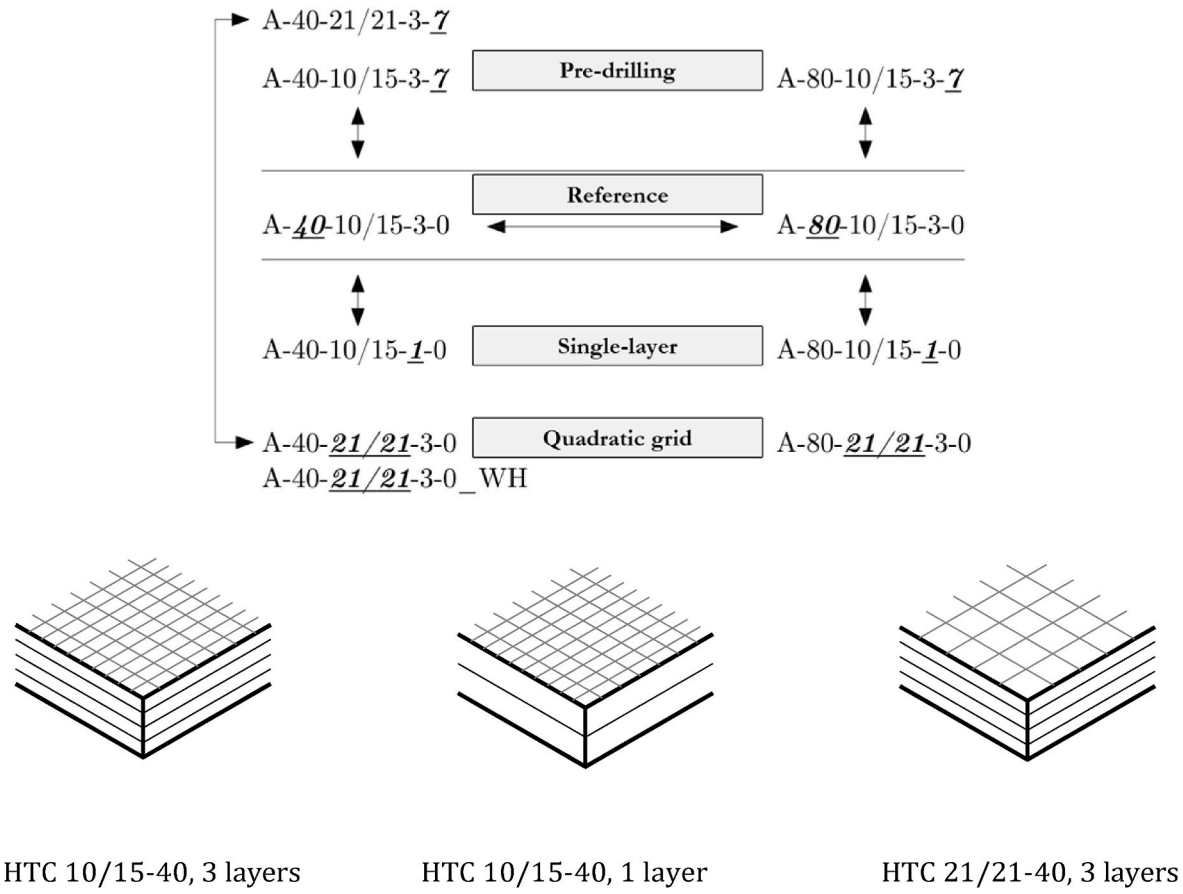

Fig. 2. (Top) Tested combinations of parameters; (bottom) Tested panel configurations.

Table 2
Fine-grained concrete mix compositions.

Ingredients/Properties	40 N/mm^2	80 N/mm^2
Cement	CEM I 32.5: 501.57 g	CEM I 42.5: 527.16 g
Water	275.84 g	210.85 g
Superplasticizer MasterGlenium ACE 460	0.80 g	4.23 g
Rhine sand 0–2 mm	1323.96 g	1391.55 g
Limestone powder Millisil W12	137.93 g	212.72 g
w/c-value	0.55	0.40
Superplasticiser/cement in wt.%	0.16	0.80

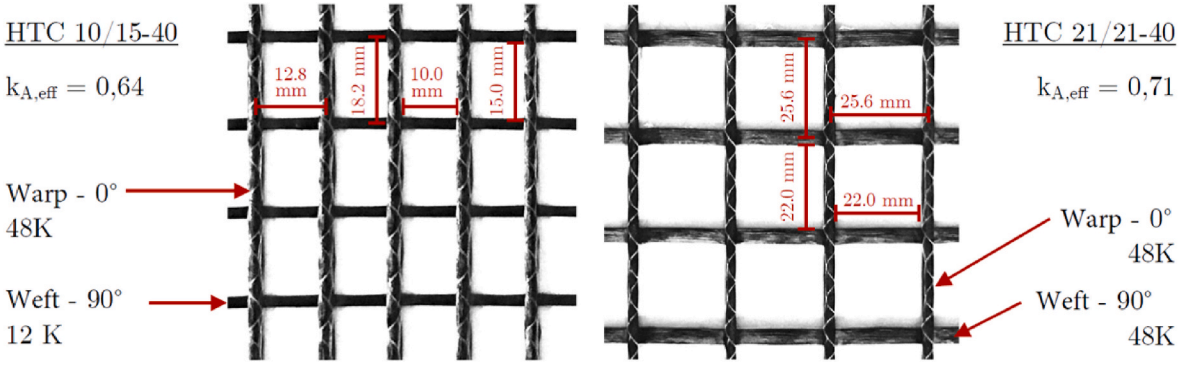

Fig. 3. Properties of textile reinforcement types HTC 10/15–40 and HTC 21/21-40.

Fig. 4. Aspects of preparation of TRC panels and material testing prisms.

Table 3
Concrete mix compositions of the used specimens.

Target concrete strength	Predrilling	Adjustment	Approx. Setting energy (Joules) [Hilti Corporation, 2021]
40 N/mm2	Yes	Green 3.0	150
40 N/mm2	No	Red 1.0	175
80 N/mm2	Yes	Yellow 3.0	200
80 N/mm2	No	Red 2.5	225

construction, which also acts as a resistance boundary for the load. When the plate is pressed under the wood girders due to the tensile load, two approximately symmetrical line supports are created on either side. The positioning of the plate is done in a way that it is subjected to bending in a 90° direction. The metal adapter is connected to the cylinder's piston, with two through-pins which resist rotation. The tensile force is introduced into the nail connection by a displacement-controlled upward movement at 0.02 mm per second. The applied load and the displacement of the nail head in relation to the concrete surface are measured hydraulically on the load cell and by use of LVDT's respectively.

3. Results and discussion

Observing the installation and pull-out test results, a comparison of the different substrate configurations is made in terms of safety and the most efficient combination of fastening parameters is determined with respect to panel strength and reinforcement type, as well as the implementation of pilot predrilling. For the selection of the most efficient configuration in terms of efficiency and safety, besides the average load resistance, the scatter of results but also the optical damage are accounted for, which reflect the structural reliability and the feeling of safety respectively. A comparative evaluation of the nail setting performance and the respective load-bearing capacity of the nail is also carried out.

3.1. Nail setting performance

Once the nails were installed according to the procedure described above, the setting quality was recorded as a first significant output of the tests. The setting quality and, respectively the defects were classified in four categories for each side of the panel, i.e. the fastening side and the fixture-free side (which may also be considered as the internal and the external/visible side of the panel respectively). This classification was based on a qualitative visual criterion as presented in Table 4 and Fig. 7 exemplarily illustrates the damage corresponding to the quality/defect classes. In order to identify the crack patterns, even for hairline cracks, a water solution was spread on both surfaces of the panel and the visible cracks' moist traces were marked. The maximum crack widths on either panel side were located and measured by means of a crack loupe magnifier with an accuracy of 0.02 mm. To filter-out any crack creep, all crack magnifier measurements were taken immediately prior to nail load testing. In addition to cracks, the nail setting can cause damage in the form of spalling around the nail on the fastening side, or in the form of circular cracking (i.e. conjectured spalling) on the fixture-free side, at the rear of the nail position. Spalling in the local area under the metal adapter was not visible and neglected. Installation quality statistics with regards to each test series are shown in the graph of Fig. 8. As seen, cases without any indications of damage (class 0) are only observed occasionally and only on the fastening side of the panel. Class 1 dominates the installation assessment in all assessments of the fastening side and some of the fixture-free side. The most severe surface defects of the panels due to nail installation are observed for the fixture free side, and for the test specimens with a single-layer textile A-40-10/15-1-0, A-80-10/15-1-0, as well as A-80-10/15-3-7, and A-80-21/21-3-0 (see also Fig. 8). At the fastening side, severe spalling was observed in only 1 out of 55 evaluated tests, but without a complete loss of the respective nail's bearing capacity. Defects of class 2 and 3 on the fixture-free side occurred in overall 29 of 55 evaluated settlements. In general, defects on the fixture-free face were characterised by a circular crack in the centre of the panel and in some cases, some centrally located unevenness, as the material is pressed slightly outwards from the nail on the other side. A fall-out of concrete fragments did not occur. There is no strict correlation of the defect classes for the two sides of the panels, i.e. each class can

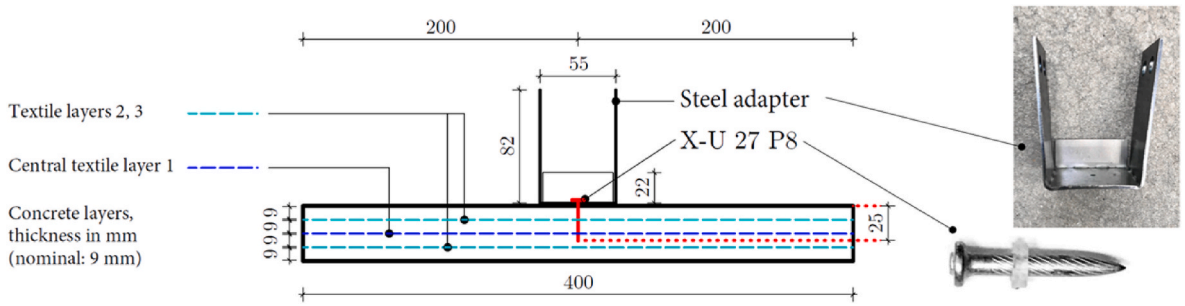

Fig. 5. Details of specimen.

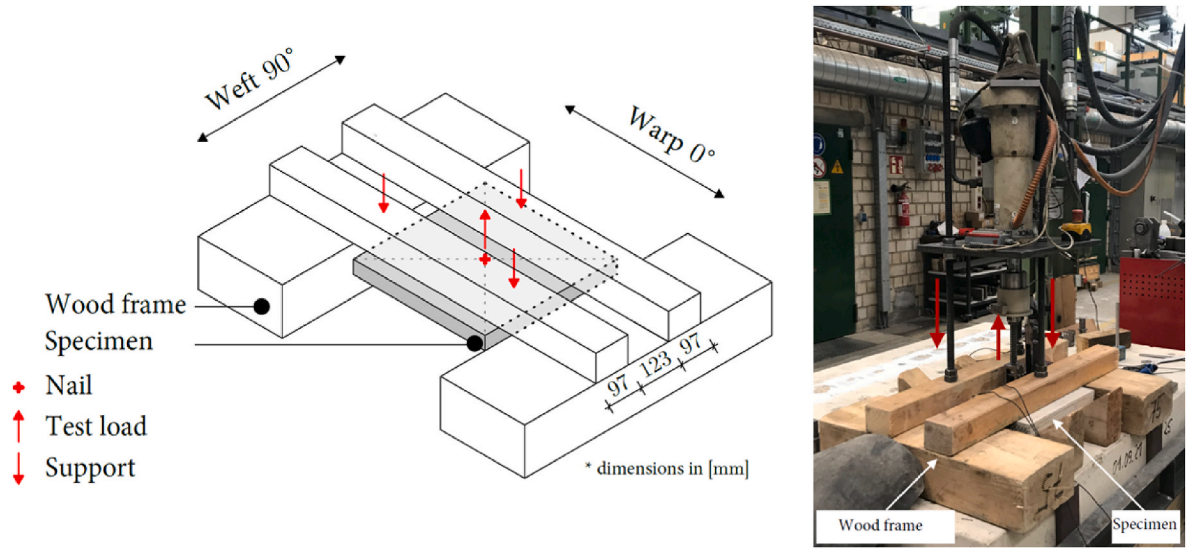

Fig. 6. Schematic representation of test configuration (left) and photo of the actual test-setup (right).

develop independently for each panel side. However, it is evident that the least overall damage was related to series A-40-10/15-3-0, as well as A-40-21/21-3-0 and its repetition A-40-21/21-3-0_WH (Fig. 8). Although this is counter-intuitive, the specific predrilling of 4 mm diameter and 7 mm depth carried out in these studies does not appear to consistently influence the nail installation quality positively or negatively in terms of defects on the panels.

With regards to the crack pattern, an additional distinction was carried out. The following two features characterise the crack patterns (See also Fig. 9).

- Crack pattern A: Cracks running perpendicularly to the panel edges, following the weak orthotropic direction of the textile, parallel or quasi-parallel to warp. There is one prominent crack with a large crack width since it absorbs the component of all strains in the panel.
- Crack pattern B: Cracks starting radially from the nail in different angles, possibly - but not necessarily - including cracks in the orthotropic directions. The crack pattern appears more uniform also with regard to the crack widths.

The crack pattern A was predominantly evident in rectangular textile configurations (73% of all cases), whilst pattern B governed panels with a quadratic textile configuration (83% of all cases). For the predrilling tests alone, these quotas change slightly, but overall the influence of predrilling in both cases does not appear to determine the cracking pattern. Panels with a single textile layer exhibited an overall maximum crack width of 0.40 mm, while panels with three layers had a maximum crack width of 0.22 mm for crack pattern A and 0.16 mm for crack pattern B.

3.2. Load resistance

As regards the maximum load, it is evident that quadratic textile configurations and high concrete strength values can achieve the overall highest average and maximum loads. As seen in Fig. 10, the highest average pull-out forces were achieved with the higher-strength concrete mix and the textile HTC 21/21–40 (A-80-21/21-3-0), while the absolute highest load capacity of a nail was also observed in this test batch with 7.29 kN. The minimum loads were 1.58 kN and 1.77 kN for the low and high-strength batches with a single rectangular grid layer, respectively.

The standard deviation values in the same figure show that the test batch with the smallest scatter of results is the one with the lower strength quadratic textile parameters (A-40-21/21-3-0). In this case, the mean value reached 4.92 kN, the standard deviation is 0.17 kN (equivalent to a variation coefficient CoV = 3.5%), while the ones for the set with higher concrete strength and the same textile arrangement are respectively 5.43 kN and 1.56 kN (CoV = 28.7%). To increase confidence in the results a repetition set consisting of 6 single tests with the same parameters was carried out (A-40-21/21-3-0_WH), yielding a slightly lower mean value of 4.37 kN and higher standard deviation of 0.52 kN (CoV = 12.0%), and similar installation quality. In this case, the mean and standard deviation values are at the same levels as those of the same test set up with predrilling, i.e. 4.22 kN and 0.47 kN (CoV = 11.2%) respectively, yet with a worse performance in terms of setting quality. The predrilling leads, however, to a mild increase in the load resistance of the nails in rectangular textile reinforcement configurations. In all cases, it is confirmed that results from panels with quadratic reinforcement yield more favourable fastening load-bearing performance compared to rectangular reinforcement layouts. Finally, panels with one layer of textile, and hence less reinforcement cross-sectional area, exhibit a lower overall resistance of up to approximately 30% as shown by comparison of the rectangular reinforcement test series A-40-

Table 4
Characteristics of defect classes.

Quality/Defect class	Fastening side of panel	Fixture-free side of panel
0	No damage	No damage
1	Cracking	Cracking
2	Cracking, spalling but firm fastening	Linear and circular cracking
3	As above but loose parts	As above but with surface spalling/flaking-off

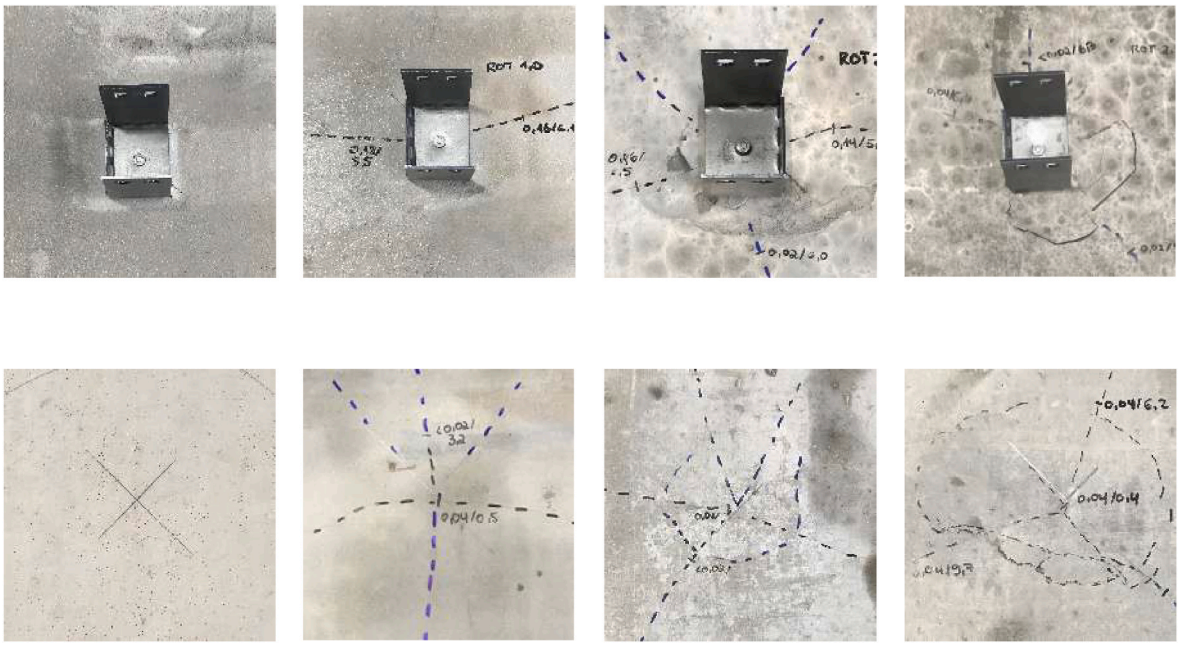

Fig. 7. Damage images of classes 0 (left), 1 (centre-left), 2 (centre-right) and 3 (right) on both the fastening (top) and the fixture-free side (bottom).

10/15-3-0 and A-80-10/15-3-0 to A-40-10/15-1-0 and A-80-10/15-1-0.

3.3. Interactions between spalling, cracking and load resistance

As noted in the previous sections, it is quite unlikely to avoid even minor cracking or local damage around the nail during installation. As shown in Fig. 11, the defect class on the fastening side correlates clearly with the pull-out loads, as it exhibits higher mean values and smaller scatter when installation defects decrease. On the contrary, defects on the fixture-free face do not influence the load resistance of the nail, understandably because the load-bearing area is mainly at the shank perimeter. The graph also distinguishes the load resistance of nails associated to the two different crack patterns (CP) A and B. Here it is made evident that nails in a single crack (CP A), carry an approximately 25% lower load compared to nails in panels with a pattern B of radial cracking. In this representation, it is also interestingly noticed that nails with a crack pattern B perform better even than the nails in undamaged panels (DC 0); this may imply that a mild cracking around the nail can absorb high local stresses and facilitate a better load-bearing performance in comparison to intact TRC that fully resists local damage. Still, given the very small sample size for DC 0 (n = 2), this should only be treated as a conjecture.

Fig. 12 presents the relationship between the loads (average and scatter) for each test series in relation to the average maximum crack widths at both panel sides for every test. The correlation of damage at installation with the nail ultimate pull-out load is also evident in this analysis. In particular, it is shown that, for a crack increase from approximately 0.05 mm–0.15 mm, the nail resistance drops by about 35% and 50% for lower and higher strength TRC, respectively (Fig. 12). Inversely, it is seen that nails in uniformly distributed quadratic reinforcement exhibit crack widths in the range of up to 0.10 mm, while a comparable panel with orthotropic rectangular textile reinforcement reaches a crack width of more than 0.20 mm. This graph also allows to confirm that quadratic textile arrangements lead to smaller crack widths and higher resistance loads in relation to rectangular ones, moreover with generally smaller scatter in the results. Furthermore, it is also remarked that lower-strength concretes generally lead to smaller crack widths. A respective influence of the predrilling is not clearly established; it is seen that it exerts an improvement in terms of both loads and crack widths for higher-strength concrete (see A-80-10/15-3-7 in comparison to the reference), i.e. the effect of predrilling needs to be considered in parallel to the concrete strength and complacency. Finally, single-layer textile reinforcement is also associated with large crack widths, which agrees with the lower pull-out resistance, as commended for Fig. 10.

3.4. Failure and post-peak characteristics

Considering the curves of the force-displacement diagrams, a great variance can be seen. Fig. 13 shows a bundle of all test load-displacement results. Regarding the load displacement curves, a rough distinction can be made between curves with a pronounced linear drop in force after reaching the ultimate load, which exhibits a rather brittle failure, and those with a stepwise reduction, indicating propagation of damage in several locations and hence some plasticity or quasi-brittleness. In all cases, failure displacements remain below 0.3 mm. Focusing on the concrete breakout shapes after nail detachment, and the detached fastening element, some distinctions can also be made. Fig. 14 presents two indicative breakout images, and four images of pulled-out nails. Upon removal of the nail, a roughly conical breakout failure was observed on the panel in all cases.

Two slightly different types of failure could be distinguished when inspecting the panel after the nail pull-out. Fig. 14a shows a conical breakout, with a partial pull-out of the nail tip from the concrete. At the same time, Fig. 14b presents a failure associated to partial detachment of the textile-concrete layer, i.e. due to excess of the interface cohesion by

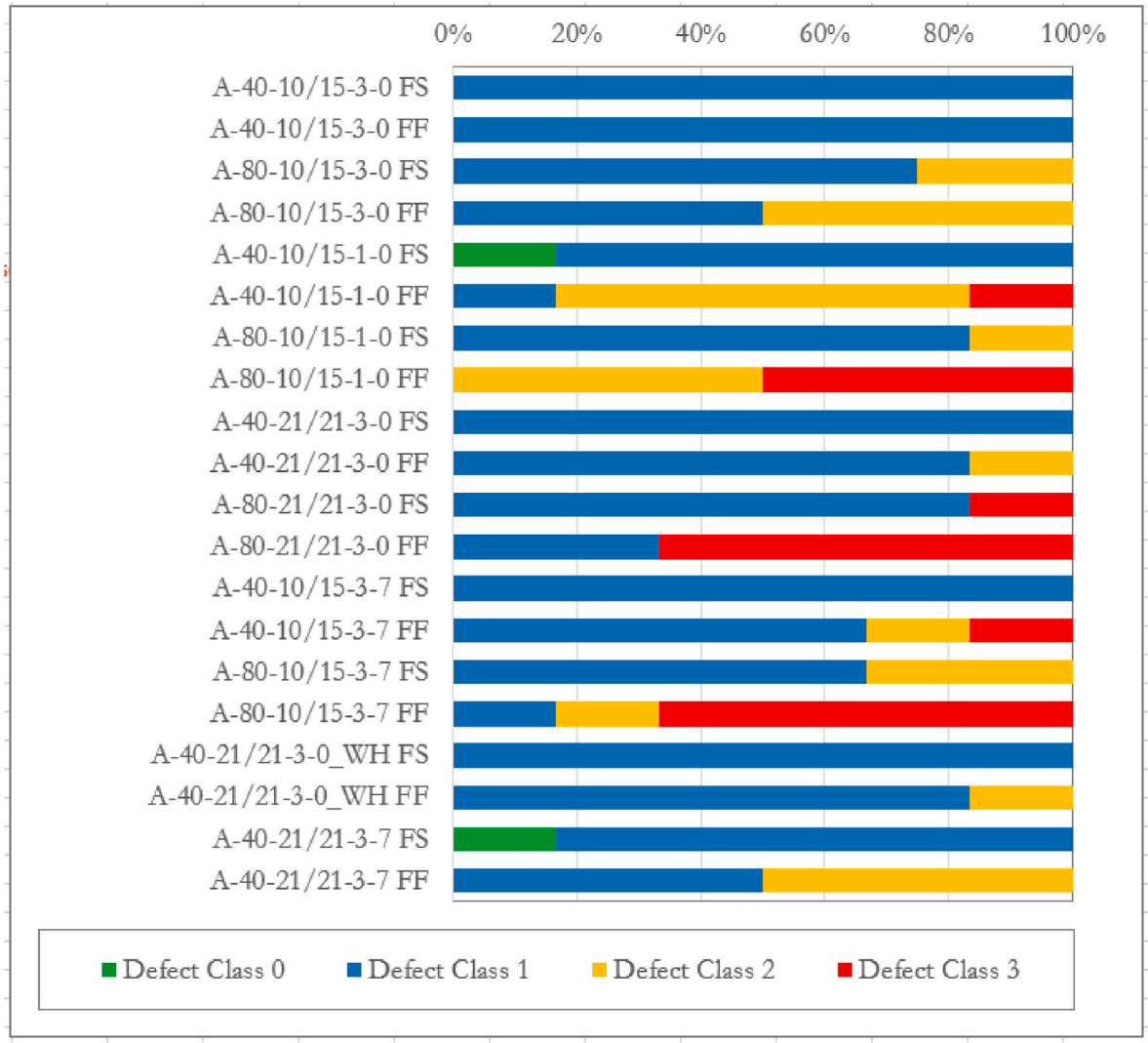

Fig. 8. Frequency of different quality/defect classes for each test series and each panel side (FS: fastening side, FF: fixture free face).

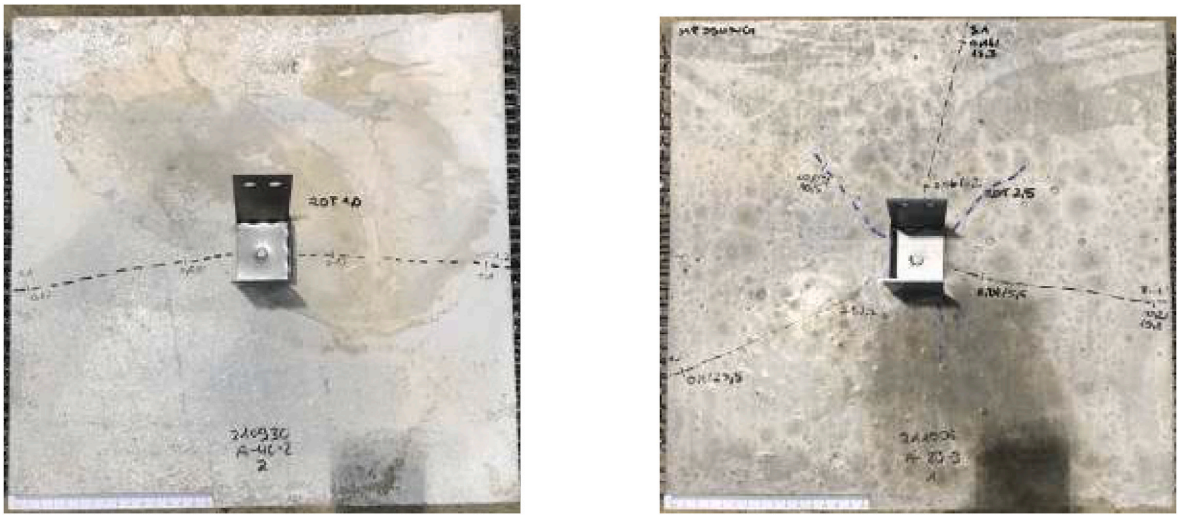

Fig. 9. Crack patterns 1-A (left), 1-B (right).

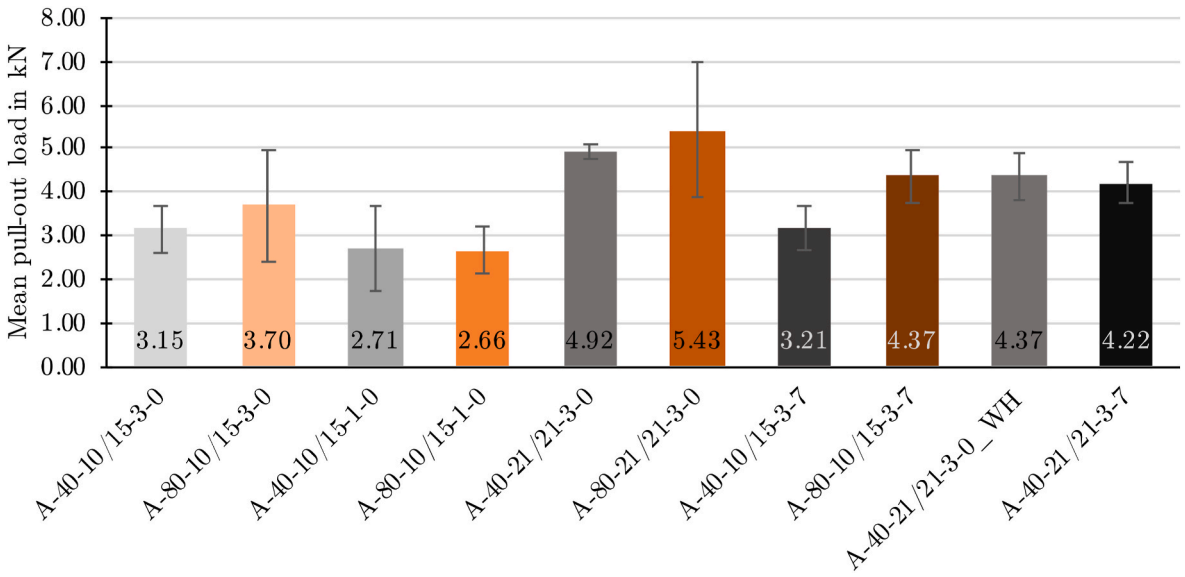

Fig. 10. Overview of the average load capacities of the nails including representation of the standard deviation.

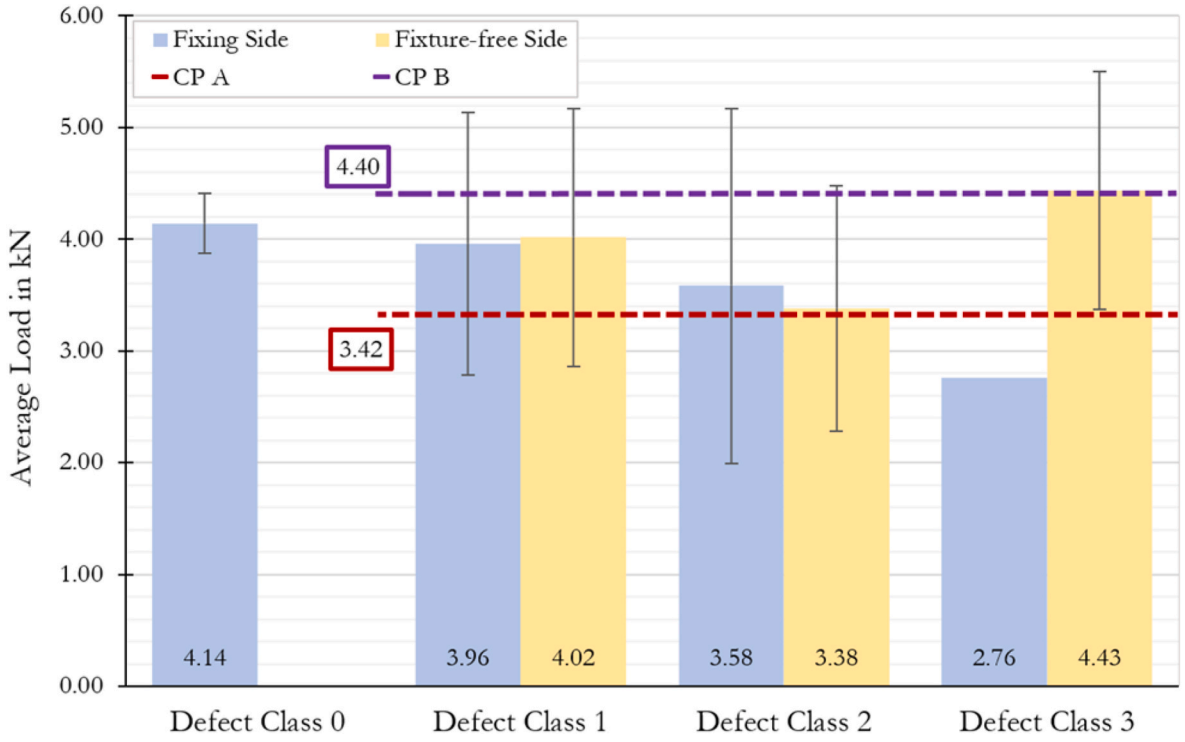

Fig. 11. Correlation of nail resistance with panel damage patterns due to installation for all tests, distinguishing the defects class on the fastenings side and the fixture free face of the panel (CP: Crack Pattern).

the locally developed normal stresses in the substrate, in the pull-out direction. An assessment of the nails following their extraction leads to a subdivision into 4 main failure body types, as shown in Fig. 14 c-f. The distinction here can be made with respect to the concrete residues on the nail shank and the shape of the breakout failure body. Fig. 14c indicates minor residues and concrete exfoliations on the shank, suggesting loss of adhesion at the nail/concrete interface. In these failure patterns a bending of the nail was also occasionally observed. Fig. 14d indicates failures with continuous residues covering the majority of the nail shank, suggesting pull-out due to friction or bond loss failure within the concrete at the perimeter of the nail. Fig. 14e presents a rhomboid shape, which is the intersection of multiple cracking planes in the substrate. Fig. 14f indicates a typical breakout failure.

Some minor correlations have been identified between the post-peak test characteristics, and the load-resistance of the nails. It is seen from Fig. 13 that brittle failures reach the highest recorded failure loads. An analysis of the samples indicates the latter two failure modes (exhibiting concrete breakout) being slightly more predominant in quadratic textile reinforcement. Besides, it is understood that the latter two failure modes (Fig. 14e and f) are related to activating a larger volume of concrete and hence leading to higher failure loads by approximately 50% as also seen in the results. Beyond these, it has not been possible to delineate a correlation of the nail resistance and the post-peak test characteristics, nor the possibility to control in advance the post-peak failure mechanism.

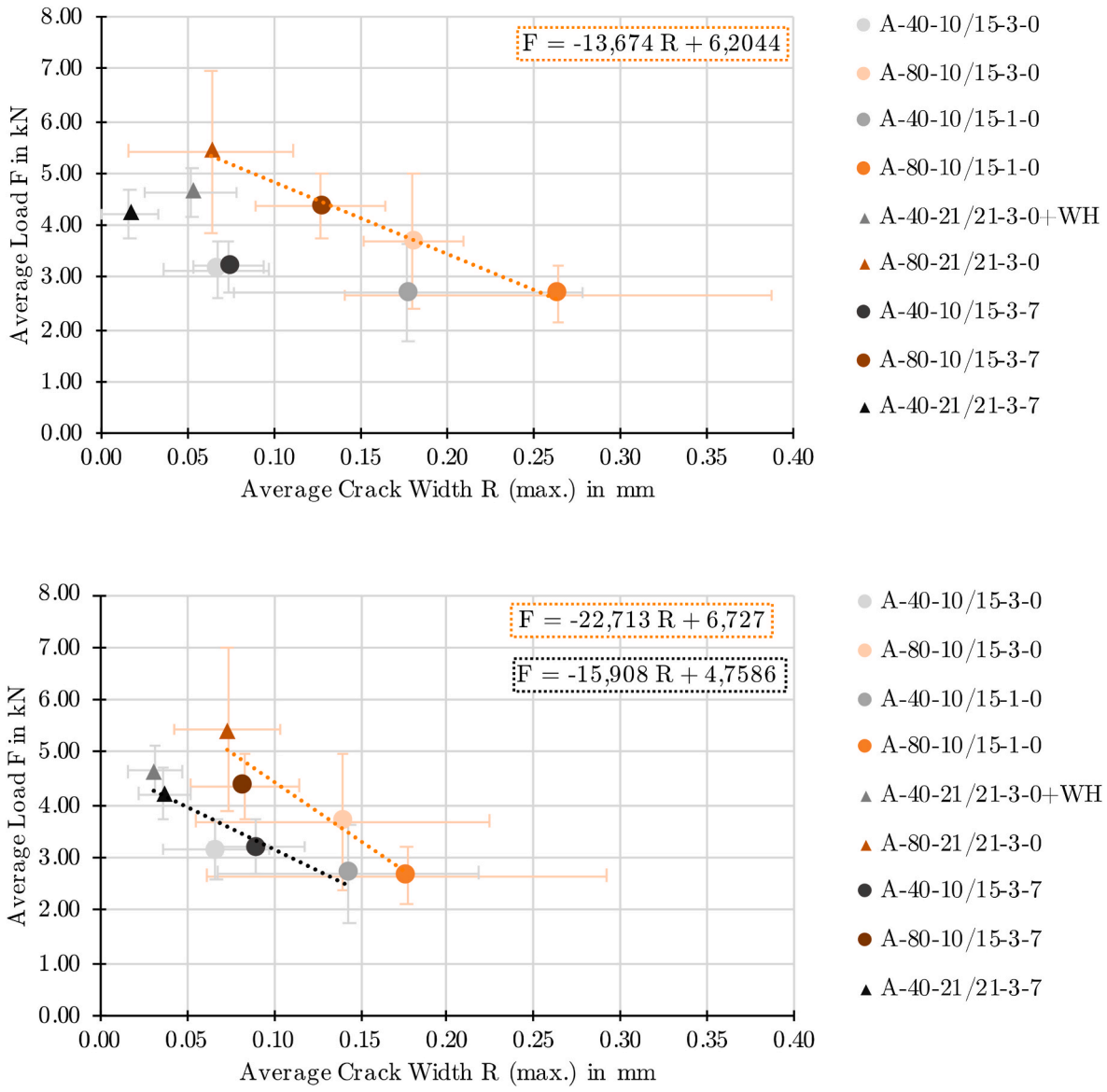

Fig. 12. Dependence of nail resistance with averaged maximum crack width from each panel side (top graph for fixture side, bottom graph for fixture free face), for all test series.

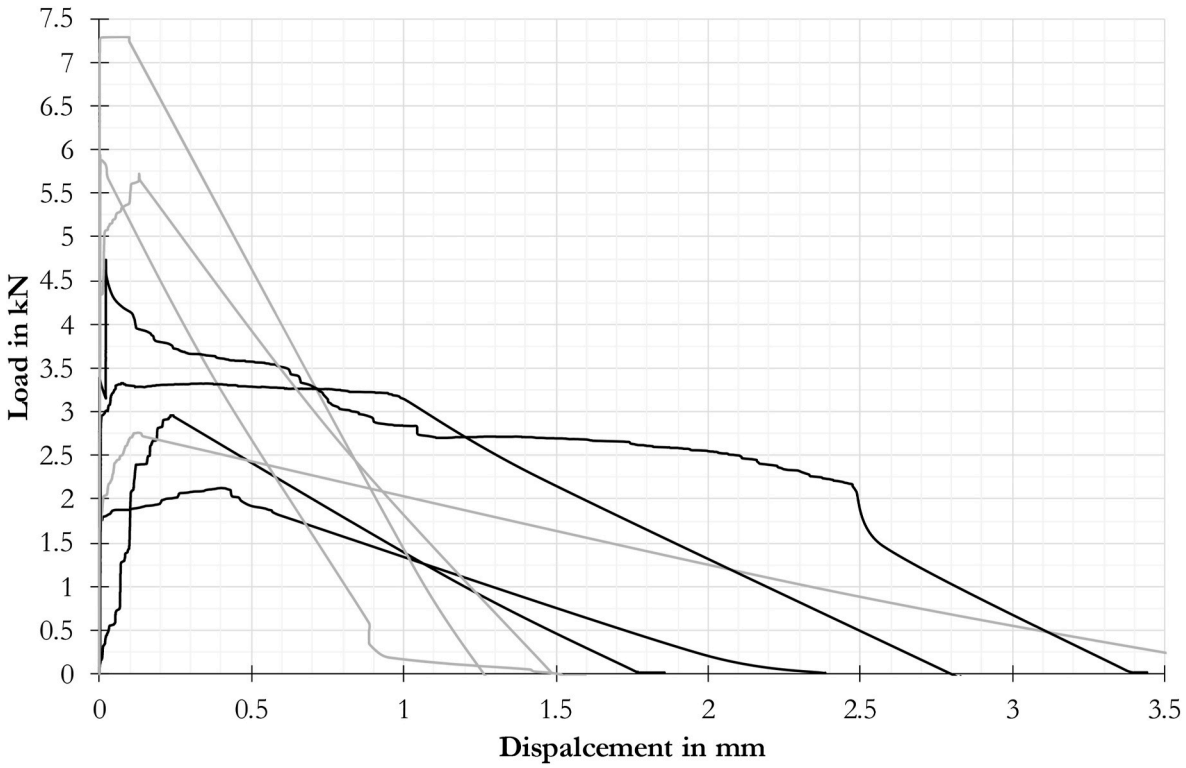

Fig. 13. Bundled representation of exemplary force-displacement diagrams of the pull-out tests; brittle load-displacement curves are plotted in light grey; dark lines show quasi-brittle load-displacement curves with post failure retention.

4. Summary of findings

In this study, the results of the investigations may be viewed and commented with respect to material, structural, and installation aspects. The most significant findings are summarised and commended below.

- An increased concrete strength positively affects the pull-out load of nails in TRC. Furthermore, it reaches overall higher values (7.29 kN) for quadratic textile configurations, which in turn implies that a uniform or isotopic layout of the reinforcement is beneficial for the expected pull-out loads.
- Nails in higher-strength concrete tend to exhibit a larger variation regarding the crack width in relation to lower-strength concrete. Furthermore, setting nails in higher strength concrete leads to installation induced damage, hence a poorer or even unacceptable appearance of the panels after nail installation.
- The formation of cracks could not be completely prevented. Specific damage patterns have been identified, which partially depend on the concrete strength and the arrangement of principal textile strength directions (rectangular/quadratic). The crack width measured due to nail installation can exceed 0.40 mm for single-layered, and it can reach 0.20–0.25 mm for 3-layered textile reinforcement. In case of the here used quadratic textile (3 layers), the crack width does not exceed 0.15 mm.
- Defects such as spalling on the fixture-free side of the panel do not influence the nail's bearing capacity but rather its appearance. Damage on the fastening side is found to be correlated with the load resistance of the nail. It may be possible that minor local cracking in more complacent, lower-strength concretes leads to relief of excessive stresses and hence allows a more stable, clamping load resistance of the nails; however, this hypothesis could not be validated. Wider cracks on both panel sides led to a reduction of fastening load-bearing capacity.
- Although some settings were sub-optimal, e.g. due to local concrete damage or nail bending, a complete elimination of the load-bearing of the nail was not observed in any case, and it remained above 1.50 kN in all tested cases. The coefficients of variations for each test series lies in the range of 3.5%–35%. In many cases, this standard deviation lies within the usual range of variations in structural concrete testing (e.g. up to 15%).
- The positive effect of pre-drilling on the setting and load-bearing performance of nails (as known from normal concrete) has not been pronouncedly identified in this study for thin plates of small-grain textile-reinforced concrete.
- The load-displacement curves exhibit an overall steep increase up to failure, with failure displacements remaining below 0.3 mm and in many cases below 0.1 mm. A quasi-brittle post-peak retention is observed occasionally.
- Irrespective of the variable test parameters, a concrete breakout is always observed during the pull-out tests. The exact typologies of post-peak behaviour and failure mode vary, but it has not been possible to derive scalable knowledge regarding the association between the nail resistance and the post-peak test characteristics.

5. Conclusion

This paper presents experimental investigations of nail fastenings in concrete panels reinforced with carbon fibre passed textile reinforcement. Varying test parameters include the concrete strength (40 and 80 N/mm^2), the textile reinforcement cross section in each direction, i.e. 1

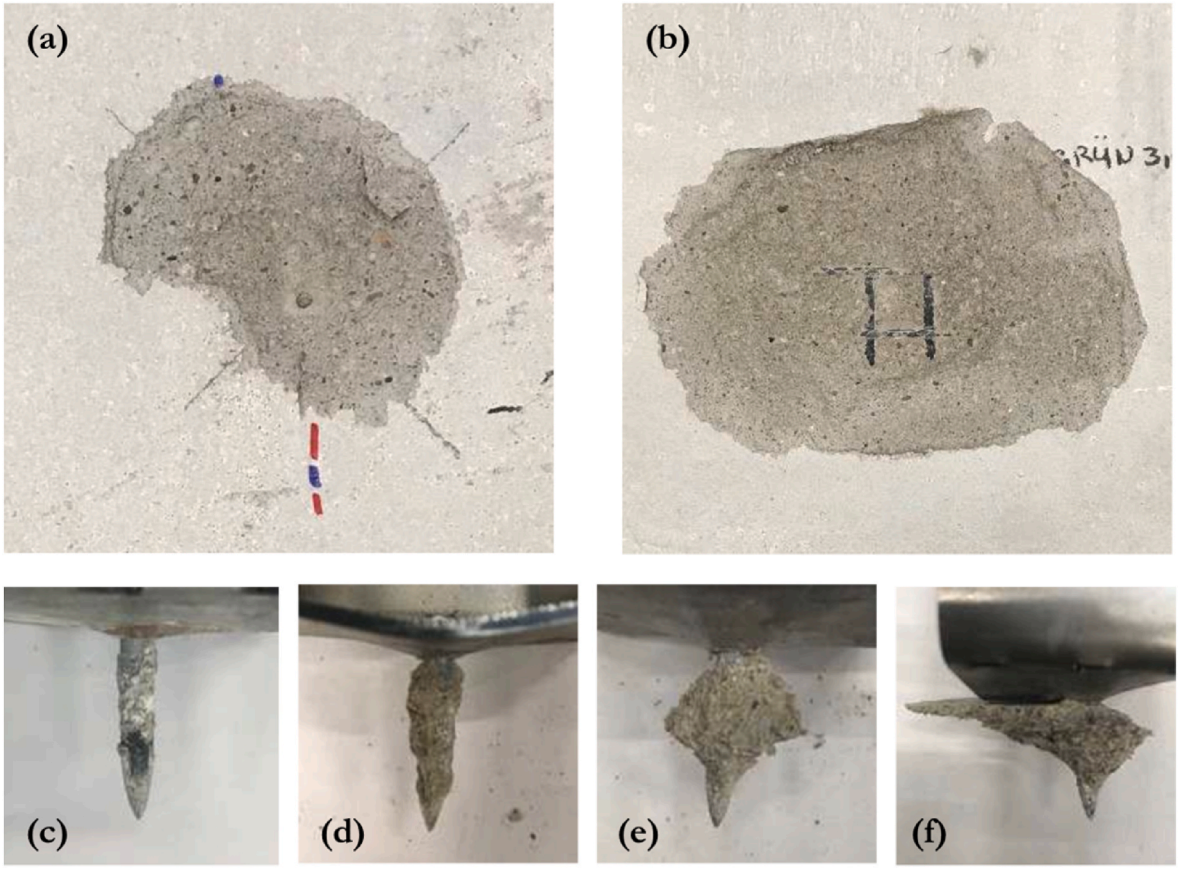

Fig. 14. Representative failure images: breakout failure as viewed on the panel fastening side (top); failure body type as viewed on the extracted nail (bottom).

and 3 layers per panel, and rectangular or quadratic textile grids installation with or without predrilling of a pilot hole. The results are used to evaluate the feasibility of this structural system for the first time in worldwide literature. Focus is drawn on the load-bearing capacity of the fastenings, the associated uncertainty, and the quality that can be achieved during installation, i.e. the defects on the panel during the impact-type nail setting. The results are focused on the axial pull-out load-bearing of the nails, the damage of the panels in terms of spalling and cracking during nail setting, and the interaction of these parameters. The post-failure performance of the system is also briefly discussed. Based on the experimental studies presented herein, it was demonstrated that the use of power actuated fastenings through nails set in TRC is in principle a feasible engineering solution, provided that the applied loads remain in the range of approximately 1.0–5.0 kN and with some tolerance on visible cracks due to installation. The investigations presented herein provide insights on this system for the first time in international literature. Based on the results, preliminary but concise guidance on the design of such systems and a roadmap for future research are offered, as outlined below.

TRC panels are in many cases, reinforced orthotropically (i.e. different strength in the weft and warp directions), but the local application of fastening pull-out loads is nearly axisymmetric. Therefore, a uniformly isotopically arranged reinforcement in panels should be considered for the load transfer. As a future development, this should be achieved e.g.by dispersed fibres or additional layers of textile reinforcement locally. For the given experimental set-up, direct fastenings without predrilling in panels with a nominal concrete strength of 40 N/mm^2 with a triple-layer quadratic textile reinforcement is the most appropriate solution in terms of average load and variation. In terms of setting quality, several cracks were observed, without necessarily adversely affecting the load performance, but certainly with a negative effect on the panel's appearance. Enhancement of the nail setting quality and ultimate loads can be achieved through careful selection of the textile reinforcement and concrete mix, as well as the geometry of predrilling. The review of all results allows the conclusion that a minimum load of 2 kN per fasteners could be anticipated for nails in TRC, and this could be even increased further for favourable panel configurations and concrete compositions. This is however to be interpreted with caution due to the large scatter of results in many cases even for the laboratory environment and the brittleness of the connections' response, which leads to reduced confidence. The scatter of loads and the potential concrete material defects in the nail area due to installation advocate that a design concept based on redundancy with multiple fastenings can suit the design of fastenings for non-structural elements. Such a design can follow modern concepts of robustness, i.e. with tolerance of damage and defects whilst ensuring that the structural system has the ability to redistribute loads through alternative paths, and does not completely collapse. The effects on the panel's cracked and/or locally damaged appearance may not render direct fastenings applicable for TRC façade elements with architectural function, but it does not necessarily exclude other applications such as, for example, TRC sacrificial formwork or industrial applications. In all cases, further research exercises are required, to reliably utilise the benefits of direct fastenings in TRC.

Test series	Cube compressive strength (N/mm^2)	Flexural strength (N/mm^2)	Test Sr. Nr. (internal)	Maximum crack width at fastening side (mm)	Maximum crack width at fixture free face (mm)	Crack pattern	Defect class	Ultimate axial load (kN)	Mean value (kN)	Standrad dviation (kN)	CoV (−)
A-40–10/15-3-0	Standard curing:	Standard curing:	2_R1.0	0.10	0.06	A	1–1	2.72	3.15	0.57	0.180
	40.17	8.32	3_R1.0	0.04	0.10	A	1–1	2.99			
	Simple indoor storage:	Simple indoor storage:	4_R1.0	0.06	0.04	A	1–1	4.14			
	38.43	6.17	5_R1.0	*0.08*	*0.08*	B	1–1	2.87			
			6_R1.0	*0.22*	*0.06*	A	1–1	3.03			
A-80–10/15-3-0	Standard curing:	Standard curing:	*2_R2.0*	*0.2*	*0.02*	*A*	*2–1*	*3.78*	3.76	0.75	0.200
	81.81	12.64	*4_R2.0*	*0.12*	*0.06*	*A*	*1–1*	*3.88*			
	Simple indoor storage:	Simple indoor storage:	5_R2.5	0.16	0.08	A	1–2	2.78			
	74.77	10.2	6_R2.5	0.2	0.20	A	1–2	4.61			
A-40–10/15-1-0	Standard curing:	Standard curing:	1_R1.0	0.26	0.18	A	1–2	1.58	2.71	0.94	0.348
	42.62	9.01	2_R1.0	0.22	0.16	A	1–2	1.96			
	Simple indoor storage:	Simple indoor storage:	3_R1.0	0.26	0.26	A	1–2	2.77			
	36.84	5.52	4_R1.0	0.12	0.12	B	1–2	3.67			
			5_R1.0	0.2	0.10	A	1–1	2.33			
			6_R1.0	0	0.04	B	0–3	3.95			
A-80–10/15-1-0	Standard curing:	Standard curing:	1_R2.5	0.40	0.16	B	1–3	2.96	2.68	0.49	0.183
	81.25	12.53	2_R2.5	0.2	0.16	B	1–3	*2.77*			
	Simple indoor storage:	Simple indoor storage:	3_R2.5	0.3	0.16	A	2–2	1.77			
	72.06	8.2	4_R2.5	0.18	0.08	B	1–3	3.01			
			5_R2.5	0.40	0.04	A	1–2	2.51			
			6_R2.5	0.10	0.10	B	1–2	3.07			
A-40–21/21-3-0	Standard curing:	Standard curing:	1_R1.0	0.06	0.06	B	1–1	4.74	4.92	0.17	0.035
	39.83	8.02	2_R1.0	0.06	0.04	B	1–1	4.74			
	Simple indoor storage:	Simple indoor storage:	3_R1.0	0.04	0.02	A	1–1	4.90			
	38.12	5.06	4_R1.0	0.08	0.04	A	1–2	4.94			
			5_R1.0	0.10	0.04	B	1–1	5.20			
			6_R1.0	0.06	0.06	B	1–1	4.99			
A-80–21/21-3-0	Standard curing:	Standard curing:	1_R2.5	0.02	0.02	B	1–3	4.66	5.43	1.56	0.287
	80.85	12.14	2_R2.5	0.12	0.10	B	1–3	5.95			
	Simple indoor storage:	Simple indoor storage:	3_R2.5	0.10	0.10	B	3–1	2.76			
	74.27	7.54	4_R2.5	0.10	0.08	B	1–3	5.72			
			5_R2.5	0.02	0.08	B	1–1	7.29			
			6_R2.5	0.02	0.06	B	1–3	6.19			
A-40–10/15-3-7	Standard curing:	Standard curing:	1_GR3.0	0.08	0.08	A	1–2	3.24	3.21	0.51	0.158
	40.04	8.35	2_GR3.0	0.10	0.08	A	1–1	3.33			
	Simple indoor storage:	Simple indoor storage:	3_GR3.0	0.08	0.14	A	1–1	2.82			
	37.44	5.24	4_GR3.0	0.04	0.06	A	1–1	3.08			
			5_GR3.0	0.08	0.08	B	1–3	4.11			
			6_GR3.0	0.06	0.10	A	1–1	2.67			

(*continued on next page*)

(*continued*)

Test series	Cube compressive strength (N/mm^2)	Flexural strength (N/mm^2)	Test Sr. Nr. (internal)	Maximum crack width at fastening side (mm)	Maximum crack width at fixture free face (mm)	Crack pattern	Defect class	Ultimate axial load (kN)	Mean value (kN)	Standrad dviation (kN)	CoV (−)
A-80–10/15-3-7	Standard curing:	Standard curing:	1_G3.0	0.12	0.14	A	1–1	5.43	4.37	0.61	0.141
	79.03	12.96	2_G3.0	0.08	0.10	A	2–3	4.26			
	Simple indoor storage:	Simple indoor storage:	3_G3.0	0.16	0.06	B	2–3	4.72			
	70.96	7.11	4_G3.0	0.12	0.08	A	1–3	3.88			
			5_G3.0	0.10	0.06	A	1–3	3.79			
			6_G3.0	0.18	0.06	A	1–2	4.14			
A-40–21/21-3-0_WH	Standard curing:	Standard curing:	1_R1.0	0.04	0.02	B	1–1	4.41	4.37	0.52	0.120
	37.66	8.75	2_R1.0	0.08	0.02	B	1–1	3.51			
	Simple indoor storage:	Simple indoor storage:	3_R1.0	0.02	0.02	B	1–1	5.13			
	35.99	4.47	4_R1.0	0.02	0.02	B	1–1	4.43			
			5_R1.0	0.04	0.02	A	1–1	4.53			
			6_R1.0	0.02	0.02	B	1–2	4.20			
A-40–21/21-3-7	Standard curing:	Standard curing:	1_GR3.0	0	0.04	B	0–1	4.33	4.22	0.47	0.112
	36.11	8.66	2_GR3.0	0.02	0.02	B	1–2	4.29			
	Simple indoor storage:	Simple indoor storage:	3_GR3.0	0	0.02	B	1–2	3.63			
	36.15	4.67	4_GR3.0	n.a.	0.04	B	1–2	4.97			
			5_GR3.0	0.02	0.04	A	1–1	3.79			
			6_GR3.0	0.04	0.06	B	1–1	4.32			

Declaration of competing interest

The authors declare that they have no known competing financial interests or personal relationships that could have appeared to influence the work reported in this paper.

Data availability

Data will be made available on request.

Acknowledgements

Hitexbau GmbH kindly provided the textiles used in the experimental investigations. Hilti Corporation offered the fastening tools and expendables. The laboratory of the Institute of Forming Technology and Lightweight Components of the TU Dortmund delivered the laser cutting of the metal sheet adapters. The authors express their strong appreciation to these contributing organisations and their very supportive representatives for the provision of materials and technical advice.

References

Beck, H., 2012. Aspects of long-term behaviour of power-actuated fastenings made to steel and concrete. In: Life-Cycle and Sustainability of Civil Infrastructure Systems: Proceedings of the Third International Symposium on Life-Cycle Civil Engineering (IALCCE'12). CRC Press, Vienna, Austria, p. 151. October 3-6, 2012.

Beck, H., Siemers, M., Reuter, M., Schöffendt, E., 2019. Setzbolzen und Metallschrauben (Set bolts and metal construction screws). In: Kuhlmann, U. (Ed.), Stahlbau Kalender 2019. John Wiley & Sons, Ltd, Hoboken/New Jersey, United States, pp. 481–585 (chapter 8).

Beßling, M., Orlowsky, J., 2022. Quantification of the influence of concrete width per fiber strand on the splitting crack failure of textile reinforced concrete (TRC). Polymers 14 (3), 489.

Beßling, M., Groh, M., Koch, V., Auras, M., Orlowsky, J., Middendorf, B., 2022a. Repair and protection of existing steel-reinforced concrete structures with high-strength, textile-reinforced mortars. Buildings 12 (10), 1615.

Beßling, M., Manko, L., Orlowsky, J., 2022b. Quantification of the transversal fiber strand stiffness of textiles used in textile-reinforced concrete via Shore hardness. Buildings 12 (11), 2038.

Corporation, Hilti, 2021. Direct Fastening Technology Manual 10/2021. Hilti Corporation, Schaan, Liechtenstein. https://www.hilti.de/c/CLS_DIRECT_ FASTENING/CLS_DX_NAILS2/CLS_DX_NAILS2_POWER/r6220 (Status:19.01.2022).

Curbach, M., Jesse, F., 2009. Eigenschaften und Anwendung von Textilbeton (Specifications and Application of Textile Reinforced Concrete - TRC). Beton-Stahlbetonbau 104 (1), 9–16.

Curbach, M., Speck, K., 2008. Konzentrierte Lasteinleitung in dünnwandige Bauteile aus textilbewehrtem Beton (Concentrated load transfer in thin-walled structural members made of textile-reinforced concrete), vol. 571. German Committee for Reinforced Concrete.

Deutsches Institut für Bautechnik, 2019. Allgemeine bauaufsichtliche zulassung/ allgemeine bauartgenehmigung nr. Z- 10, 3–814 (Status:02.02.2022).

Deutsches Institut für Bautechnik, 2021a. Allgemeine Bauartgenehmigung Nr. Z-21.9-2072 (Status:02.02.2022).

Deutsches Institut für Bautechnik, 2021b. Halfen FPA-SL30 System Zulassung/ Bauartgenehmigung Z-21.8-2067 (Halfen FPA-SL30 System Approval/Type Approval Z-21.8-2067). https://www.halfen.com/de_. DE/druckschriften/ zulassungen. (Status:20.01.2022).

DIN EN 12390-2, 2019. Prüfung von Festbeton – Teil 2: herstellung und Lagerung von Probekörpern für Festigkeitsprüfungen (Testing of hardened concrete - Part 2: Production and storage of specimens for strength tests). German version EN 12390-2: 2019.

DIN EN 1015-3, 2007. Prüfverfahren für Mörtel und Mauerwerk - teil 3: bestimmung der Konsistenz von Frischmörtel (mit Ausbreittisch) (Test methods for mortar for masonry - Part 3: determination of consistency of fresh mortar (with spreading table)). German version EN, 1015-3:1999+A1:2004+A2:2006.

DIN EN 196-1, 2016. Prüfverfahren für Zement – Teil 1: Bestimmung der Festigkeit (Test methods for cement - Part 1: Determination of strength). German version EN 196-1: 2016.

EOTA (European Organisation for Technical Assessment), 2018. EAD 330083-02-0601 Powder-Actuated Fastener for Multiple Use in Concrete for Non-structural Applications, OJEU 2018/C 370/05.

Gerber, W., 1987. Theorie zum Eintreiben und Verankern von Bolzen in Beton (Theory for penetration and anchoring of bolts in concrete). Bauingenieur 62, 213–218.
Haist, M., Bergmeister, K., Curbach, M., Forman, P., Gaganelis, G., Gerlach, J., Mark, P., Moffatt, J., Müller, C., Müller, H.S., Reiners, J., 2022. Nachhaltig konstruieren und bauen mit Beton (Sustainable design and construction with concrete). BetonKalender, 2022. Nachhaltigkeit, Digitalisierung, Instandhaltung, pp. 421–531.
Hegger, J., Will, N., Schneider, H.N., Schätzke, C., Curbach, M., Jesse, F., 2005. Fassaden aus textilbewehrtem Beton (Façades made of textile-reinforced concrete). In: Beton + Fertigteil- Jahrbuch. Bauverlag BV GmbH, Gütersloh, pp. 76–82.
Hitexbau GmbH (n.D.a). Art. 279135 HTC 10/15-40. https://www.hitexbau.com/menu/products/. (Status:19.01.2022).
Hitexbau GmbH (n.D.b). HTC 21/21-40. (Status:02.02.2022).
Hoepfner, M., Spyridis, P., Bessling, M., Orlowsky, J., 2021. Experimental investigations of shallow mechanical and bonded anchors in textile reinforce concrete. In: Chen, A., Ruan, X., Frangopol, D. (Eds.), Life-Cycle Civil Engineering: Innovation, Theory and Practice, first ed. CRC Press, London, pp. 1046–1053.
Lieboldt, M., 2015. Feinbetonmatrix für Textilbeton (Fine concrete matrix for TRC). Beton- Stahlbetonbau 110 (S1), 22–28.
Lorenz, E., 2015. Endverankerung und Übergreifung textiler Bewehrungen in Betonmatrices (End anchorage and overlap of textile reinforcements in concrete matrices). Dissertation, Dresden University of Technology, Dresden.
Lorenz, E., Schütze, E., Schladitz, F., Curbach, M., 2013. Textilbeton – grundlegende Untersuchungen im Überblick (TRC - basic investigations at a glance). Beton- Stahlbetonbau 108 (10), 711–722.
Ortlepp, R., 2007. Untersuchungen zur Verbundverankerung textilbewehrter Feinbetonverstärkungsschichten für Betonbauteile (Investigations for the bond anchoring of textile reinforced fine-grained concrete strengthening layers of RC members). PhD thesis Technische Universität Dresden (Dresden).
Patzak, M., 1979. Zur Frage der Sicherheit von Setzbolzenbefestigungen in Betonbauteilen (The safely of fastenlng bolls in concrete elements). Betonw. Fertigtl. 45 (5), 308–314.
Scheerer, S., 2015. Was ist Textilbeton? Eine kurze Einführung in das Thema (What is textile concrete? A short introduction to the topic). Beton- Stahlbetonbau 110 (S1), 4–7.
Walther, T., Schladitz, F., Curbach, M., 2014. Textilbetonherstellung im Gießverfahren mit Hilfe von Abstandhaltern. (Textile concrete production in the casting process using spacers). Beton- Stahlbetonbau 109 (3), 216–222.